Supporting Information

Charge Transfer-Induced Torsional Dynamics in the Excited State of 2,6-Bis(diphenylamino)anthraquinone

Jungkweon Choi,[a,b,*] Doo-Sik Ahn,[a,b] Key Young Oang,[c] Dae Won Cho,[d] Hyotcherl Ihee[a,b,*]

a. Center for Nanomaterials and Chemical Reactions, Institute for Basic Science, Daejeon 34141, Republic of Korea.
b. Department of Chemistry, KAIST, Daejeon 34141, Republic of Korea.
c. Radiation Center for Ultrafast Science, Quantum Optics Division, Korea Atomic Energy Research Institute (KAERI), Daejeon 34057, Republic of Korea.
d. Department of Advanced Materials Chemistry, Korea University, Sejong Campus, Sejong 30019, Korea.

*Corresponding author: Jungkweon Choi, Hyotcherl Ihee

E-mail: jkchoi@ibs.re.kr, hyotcherl.ihee@kaist.ac.kr

Experimental Section

The 2,6-bis(diphenylamino)anthraquinone (DPA-AQ-DPA) was purchased from Tokyo Chemical Industry (TCI) Co., Ltd. and used without further purification. Cyclohexane, diethyl ether, and THF were purchased from Sigma-Aldrich. Acetonitrile (MeCN) and *n*-hexane were purchased from Junsei Chemical Co. CH_2Cl_2 was purchased from TCI Co. All solvents were used without further purification.

Spectroscopic measurements: The steady-state UV-visible absorption and emission spectra of DPA-AQ were measured using a Shimadzu UV-2600 and FL spectrometer LS 55 (PerkinElmer), respectively. The sub-picosecond time-resolved absorption spectra were collected using a pump–probe transient absorption spectroscopy system. The pump light was generated by using a regenerative amplified titanium sapphire laser system (Spectra Physics, Spitfire Ace, 1 kHz) pumped by a diode-pumped Q-switched laser (Spectra Physics, Empower). The seed pulse was generated using a titanium sapphire laser (Spectra Physics, MaiTai SP). The pulses (330 nm) generated from an optical parametric amplifier (Spectra Physics, TOPAS prime) were used as the excitation beam. A white light continuum pulse, which was generated by focusing the residual of the fundamental light to a thin sapphire crystal after the controlled optical delay, was used as a probe beam and directed to the sample cell with 2.0 mm of the optical path. The transmitted probe beam was detected with a CCD detector installed in the absorption spectroscope. The pump pulse was chopped by the mechanical chopper synchronized to one-half of the laser repetition rate, resulting in a pair of the spectra with and without the pump, from which the absorption change induced by the pump pulse was estimated.

Singular value decomposition (SVD) analysis: In order to determine the kinetic model, it is necessary to examine how many distinct transient species are involved in the dynamic process of interest and how fast the population of each species changes after photoexcitation. For this purpose, we applied the SVD analysis and kinetic analysis, which will be detailed in the next section, to our experimental data in the λ range of 450–750 nm. From the experimental TA spectra measured at various time delays, we can build an $n_\lambda \times n_t$ matrix **A**, where n_λ is the number of λ points in the TA spectrum at a given time-delay point (301 wavelength points for DPA-AQ-DPA in MeCN and diethylether) and n_t is the number of time-delay points (255 time delay points in the wavelength range from 450 nm to 750 nm for DPA-AQ-DPA in MeCN and diethylether). Then, the matrix **A** can be decomposed while

satisfying the relationship of $\mathbf{A} = \mathbf{USV}^{T}$, where **U** is an $n_\lambda \times n_t$ matrix whose columns are called left singular vectors (lSVs) (i.e. time-independent λ spectra) of **A**, **V** is an $n_t \times n_t$ matrix whose columns are called right singular vectors (rSVs) (i.e. amplitude changes of **U** as time evolves) of **A**, and **S** is an $n_t \times n_t$ diagonal matrix whose diagonal elements are called singular values of **A** and can possess only non-negative values. The matrices **U** and **V** have the properties of $\mathbf{U}^{T}\mathbf{U} = \mathbf{I}_{nt}$ and $\mathbf{V}^{T}\mathbf{V} = \mathbf{I}_{nt}$, respectively, where $\mathbf{I}_{nt}$ is the identity matrix. Since the diagonal elements (i.e. singular values) of **S**, which represent the weight of left singular vectors in **U**, are ordered so that $s_1 \geq s_2 \geq \cdots\cdots \geq s_n \geq 0$, (both left and right) singular vectors on more left are supposed to have larger contributions to the constructed experimental data. In this manner, we can extract the time-independent transient absorption components from the lSVs and the time evolution of their amplitudes from the rSVs. The former, when combined together, can give the information on the TA spectra of distinct transient species, while the latter contains the information on the population dynamics of the transient species.

The singular values and autocorrelations of the corresponding singular vectors suggest that the first n_p singular vectors are enough to represent our experimental data because the contribution of each singular vector (lSV or rSV) to the data is proportional to its corresponding singular value and the autocorrelation of **U** or **V** matrix can serve as a good measure of signal-to-noise ratio of the singular vectors (in this study, four and five significant singular components for the data of DPA-AQ-DPA in MeCN and diethylether, respectively). In other words, the contribution from the $(n_p + 1)_{th}$ singular vectors and beyond becomes negligible. In this regard, the first n_p rSVs multiplied by singular values were fit by a sum of multiple exponentials sharing common relaxation times.

Kinetic analysis: Using the first a few singular vectors of significant singular values (that is, n_p principal singular vectors) obtained from the SVD analysis of the experimental data, we performed kinetic analysis. New matrices, **U**', **V**', and **S**', can be defined by removing non-significant components from **U**, **V**, and **S**, respectively. In other words, **U**' is an $n_\lambda \times n_p$ matrix containing the first n_p left singular vectors of **U**, **V**' is an $n_t \times n_p$ matrix containing the first n_p right singular vectors of **V**, and **S**' is an $n_p \times n_p$ diagonal matrix containing the first n_p singular values of **S**. Here we represent the time-dependent concentrations of transiently formed intermediate species, which can be calculated from a kinetic model, by a matrix **C**. Then, the matrix **C** can be related to **V**' by using a parameter matrix **P** that satisfies $\mathbf{V}' = \mathbf{CP}$, where **C** is an $n_t \times n_p$ matrix whose columns represent time-

dependent concentrations of transiently formed intermediate species and **P** is an $n_p \times n_p$ matrix whose columns contain coefficients for the time-dependent concentrations so that the linear combination of concentrations of the n_p intermediates can form the n_p right singular vectors in **V**', respectively. Once **C** is specified by a kinetic model with a certain set of variable kinetic parameters such as rate coefficients, **P** and **C** can be optimized by minimizing the discrepancy between **V**' (from the experiment) and **CP** (from the kinetic theory).

Since **V**' = **CP**, the following relationships hold:

$$\mathbf{A}' = \mathbf{U}'\mathbf{S}'\mathbf{V}'^{\mathrm{T}} = \mathbf{U}'\mathbf{S}'(\mathbf{CP})^{\mathrm{T}} = \mathbf{U}'\mathbf{S}'\mathbf{P}^{\mathrm{T}}\mathbf{C}^{\mathrm{T}} = (\mathbf{U}'\mathbf{S}'\mathbf{P}^{\mathrm{T}})\mathbf{C}^{\mathrm{T}} \qquad \text{(Eqn. S1)}$$

where **A**' is an $n_\lambda \times n_t$ matrix that contains the theoretical TA spectrum $\Delta A(\lambda_i,t_j)$ at given λ and t values. Theoretical TA spectra calculated by using Eqn. S1 were compared with the experimental TA spectra, and the matrix **P** and **C** were optimized by minimizing the discrepancy (quantified by least-square, LS) between the theoretical and experimental TA spectra using the Minuit[1] package:

$$LS = \sum_{i=1}^{n_\lambda}\sum_{j=1}^{n_t}\left\{\Delta A_{\exp}(\lambda_i,t_j) - \Delta A_{the}(\lambda_i,t_j)\right\}^2 \qquad \text{(Eqn. S2)}$$

$\Delta A_{exp}(\lambda_i,t_j)$ and $\Delta A_{the}(\lambda_i,t_j)$ are the experimental and theoretical TA spectrum at a given point of (λ_i,t_j), respectively. From Eqn. S1, we can define a matrix **B** as $\mathbf{B} = \mathbf{U}'\mathbf{S}'\mathbf{P}^{\mathrm{T}}$, that is, a linear combination of the n_p left singular vectors in **U**' weighted by their singular values in **S**' with their ratios determined by **P**. Then, the matrix **E**, an $n_t \times n_p$ matrix, contains the n_p time-independent TA spectra directly associated with the n_p intermediate species. Therefore, by optimizing the matrices P and C, we obtain both the time-dependent concentrations (see the optimized **C** for the kinetic model in Figures 5b and S4b) and the time-independent TA spectra of the intermediate species (see the optimized **P** for the kinetic model in Figures 5a and S4a).

Density Functional Theory (DFT): All DFT and TD-DFT calculations were implemented with the Gaussian09[2]. Various hybrid DFT methods were used for the calculations of optimized geometries at the single and triplet ground states. TD-DFT methods were also used for the calculation of optimized geometries and vertical/adiabatic transition energies at the excited states. The DFT methods used are specified in Tables S1 and S2.

Reference

1. James, F., “MINUIT—Function Minimization and Error Analysis,” CERN Program Library Long Writeup D506, **1972.**
2. Frisch, M. J. et al. Gaussian 09, Revision A.02 (Gaussian Inc., 2009).

Table S1. TD-DFT and DFT Calculated geometric and electronic excitation parameters for S_0, and S_1 ($CS_{twisting}$) in diethyl ether and MeCN.

	S_0 geometry in diethyl ether (in acetonitrile)				**S_1 geometry in diethyl ether (in acetonitrile)**				
	R(C-N) (Å)[a]	θ_1/θ_2 or θ (deg)[b]	E_{VA}(CT) (eV)[c]	f_{VA}[d]	R(C-N) (Å)	θ_1/θ_2 or θ (deg)	E_{VE}(CT) (eV)[e]	f_{VA}	μ (debye)[f]
B3LYP/ 6-31G(d)	1.40 (1.40)	27 (26)	2.43 (2.40)	0.454 (0.461)	1.42/1.46 (1.45/1.42)	40/77 (38/70)	1.87/1.97 (1.43/1.71)	0.0/0.424 (0.013/0.187)	22.0 (22.0)
B3LYP/ 6-31G(d) + C_i constraint	1.40 (1.40)	27 (26)	2.43 (2.40)	0.454 (0.461)	1.44 (1.43)	58/60 (52/54)	2.28/2.41 (1.61/1.63)	0.0/0.5301 (0.0/0.2584)	0.0 (0.0)
B3LYP/ 6-31G(d) HF%=28.4[g]	1.32 (1.32)	26 (26)	2.96 (2.92)	0.536 (0.543)	1.34/1.35 (1.33/1.35)	36/52 (38/52)	2.09/2.31 (1.97/2.06)	0.107/0.342 (0.0/0.4831)	18.2 (18.2)
CAM-B3LYP/ 6-31G(d)	1.40 (1.39)	26 (25)	3.31 (3.27)	0.741 (0.743)	1.40 (1.39)	36 (34)	2.60/2.87 (2.53/2.79)	(0.072/0.676) (0.087/0.697)	0.007 (0.003)
MPW1B95/ 6-31G(d)	1.39 (1.39)	28 (28)	2.68 (2.64)	0.52 (0.528)	1.41/1.43 (1.41/1.42)	42/52 (39/48)	1.96/2.11 (2.02/2.12)	(0.082/0.310) (0.0/0.5162)	17.7 (17.1)

a: C-N bond distance connecting DPA and AQ

b: Dihedral angles for CCNC angles

c: Vertical absorption energies for two lowest excited states

d: Oscillator strength

e: Vertical emission energies for two lowest excited states

f: Excited state dipole moment

g: HF%: Hartree-Fock percentage in exchange correlation functionals

Table S2. TD-DFT and DFT Calculated geometric and electronic excitation parameters for triplet state (T_1) in diethyl ether and MeCN.

	T_1 geometry in diethyl ether (in acetonitrile)			
	R(C-N) (Å)[a]	θ_1/θ_2 or θ (deg)[b]	E_{VA}(CT) (eV)[c]	f_{VA}[d]
B3LYP/ 6-31G(d)	1.41 (1.41)	35 (35)	0.25/0.82 (0.31/1.02)	0.134/0.0 (0.080/0.0001)
B3LYP/ 6-31G(d) + C_i constraint	1.41 (1.41)	35/37 (35/37)	0.82/1.03 (0.05/0.96)	0.0/0.0002 (0.1999/0.0)
B3LYP/ 6-31G(d) HF%=28.4[e]	1.32/1.33 (1.32/1.33)	34/35 (35/36)	0.59/1.67 (0.76/1.70)	0.055/0.009 (0.041/0.043)
CAM-B3LYP/ 6-31G(d)	1.39/1.41 (1.39)	32/36 (30/34)	1.45/1.61 (1.63/1.65)	0.0418/0.098 (0.029/0.082)
MPW1B95/ 6-31G(d)	1.40 (1.40)	32/34 (32/34)	0.13/1.06 (0.15/1.20)	0.1491/0.0 (0.1567/0.0)

a: C-N bond distance connecting DPA and AQ

b: Dihedral angles for CCNC angles

c: Vertical absorption energies for two lowest excited states

d: Oscillator strength

e: HF%: Hartree-Fock percentage in exchange correlation functionals

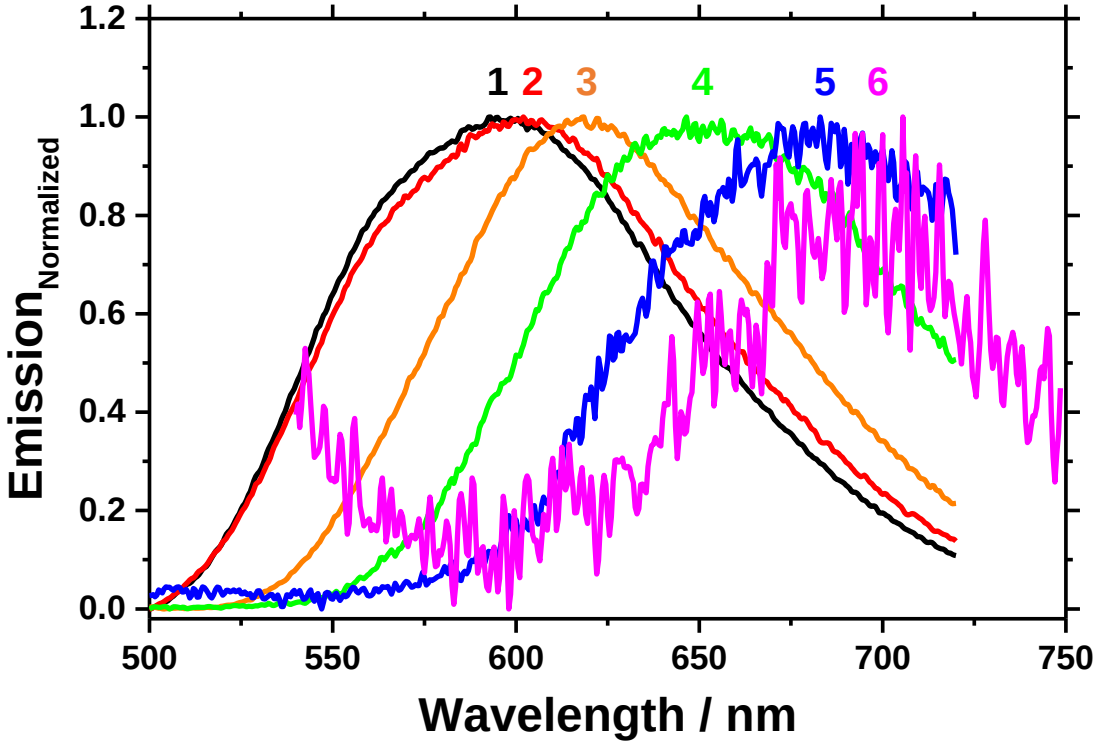

Figure S1. Normalized emission spectra of DPA-AQ-DPA measured in various solvents. (1, cyclohexane; 2, n-hexane; 3, diethyl ether; 4, THF; 5, CH_2Cl_2; and 6, MeCN). Excitation wavelength is 370 nm.

	HOMO-1 (S_0, optimized)	LUMO (S_0, optimized)	HOMO (S_1, optimized)	LUMO (S_1, optimized)
MPW1B95 /6-31G(d) In diethylether	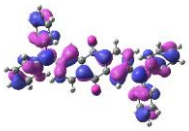	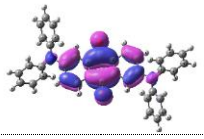	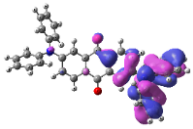	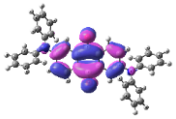
MPW1B95 /6-31G(d) In MeCN	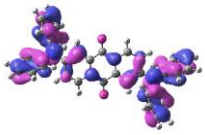	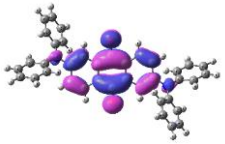	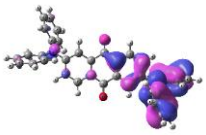	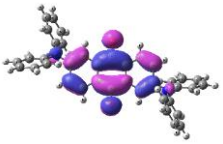
B3LYP /6-31G(d) In diethylether		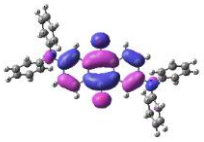	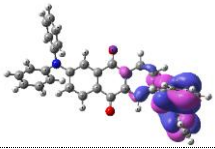	
B3LYP /6-31G(d) In MeCN		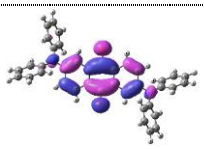	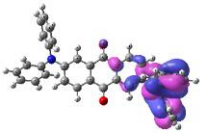	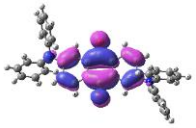

Figure S2. Calculated molecular orbitals for HOMO-1/LUMO and HOMO/LUMO pairs for S_0 and S_1 ($CS_{twisting}$) states, respectively. (Isosurface value: 0.02 eÅ^{-3})

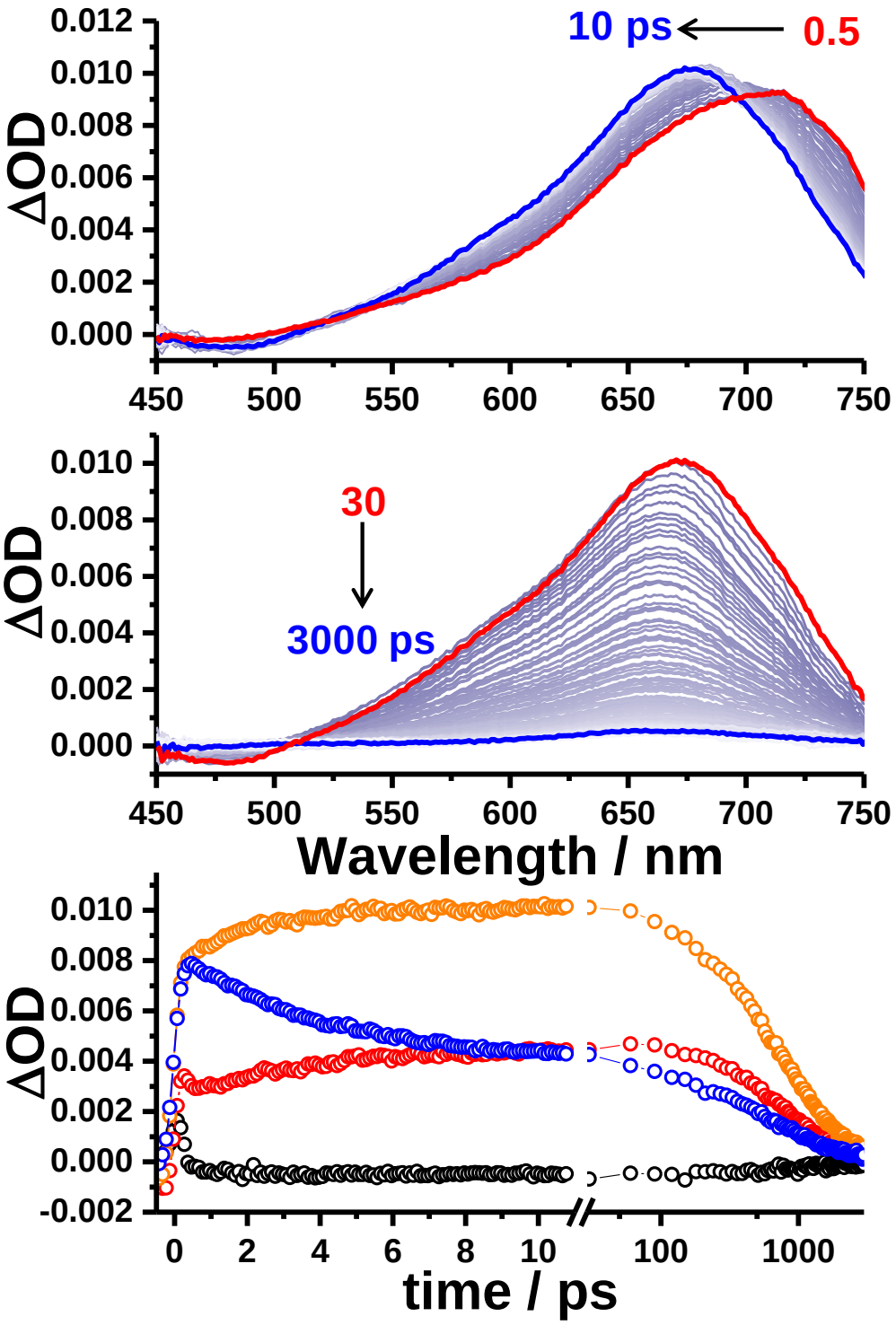

Figure S3. Top and middle) TA spectra of DPA-AQ-DPA in diethyl ether. Excitation wavelength is 330 nm. Bottom) Decay profiles monitored at selected wavelengths (○: 480 nm, ○: 600 nm, ○: 675 nm, and ○: 735 nm).

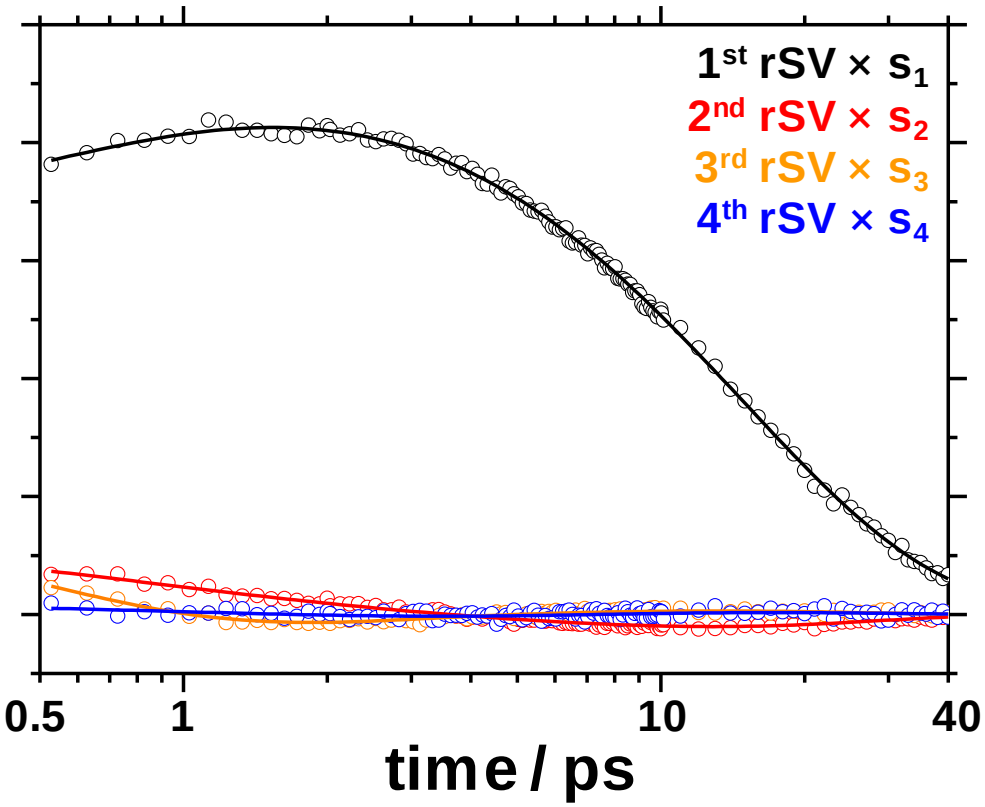

Figure S4. The first four rSVs multiplied by singular values (S_iV_i) for DPA-AQ-DPA in MeCN are shown. The first four rSVs multiplied by singular values were fit by using four exponentials sharing common time constants, yielding the time constants of 0.5 ± 0.1, 1.4 ± 0.4, 8.2 ± 4.2, and 12.9 ± 1.9 ps. Theoretical fitting curves are shown as solid lines.

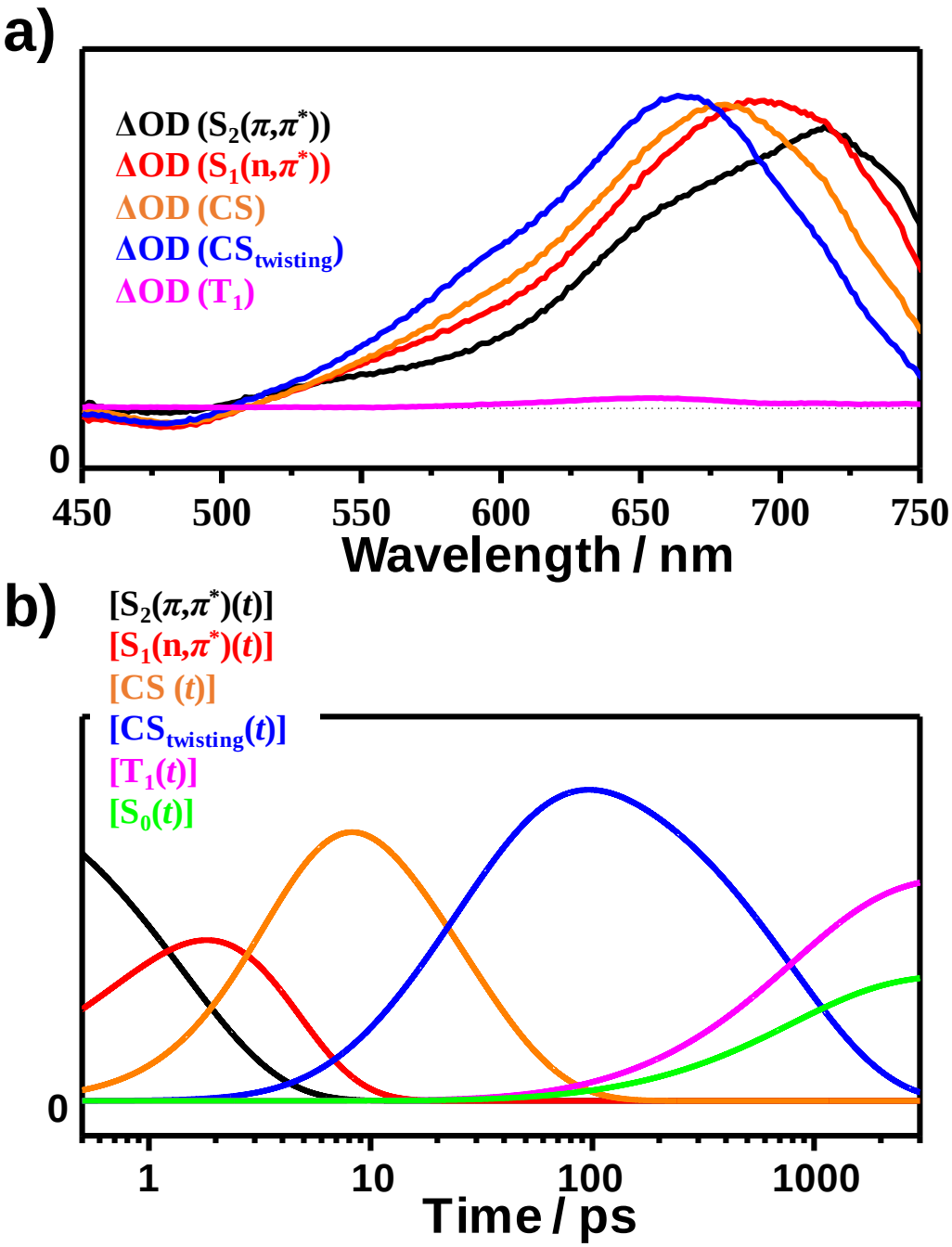

Figure S5. Species-associated spectra (a) and population changes (b) for five intermediates, $S_2(\pi,\pi^*)$, $S_1(n,\pi^*)$, CS state, $CS_{twisting}$ state, and $^3(\pi,\pi^*)$ state for DPA-AQ-DPA in diethyl ether.

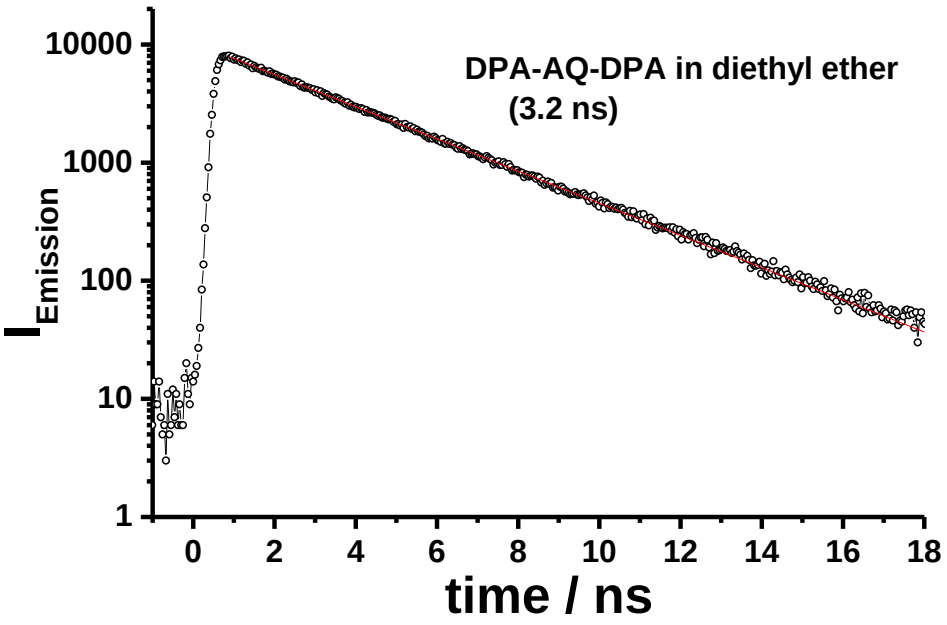

Figure S6. Emission decay profile of DPA-AQ-DPA in diethyl ether.